Multi-channel 28-GHz millimeter-wave signal generation on a silicon photonic chip with automated polarization control

Ruiyuan Cao, Yu He, Qingming Zhu, Jingchi Li, Shaohua An, Yong Zhang, and Yikai Su†

State Key Laboratory of Advanced Optical Communication Systems and Networks, Department of Electronic Engineering, Shanghai Jiao Tong University, Shanghai 200240, China

Abstract: We propose and experimentally demonstrate an integrated silicon photonic scheme to generate multi-channel millimeter-wave (MMW) signals for 5G multi-user applications. The fabricated silicon photonic chip has a footprint of 1.1×2.1 mm^2 and integrates 7 independent channels each having on-chip polarization control and heterodyne mixing functions. 7 channels of 4-Gb/s QPSK baseband signals are delivered via a 2-km multi-core fiber (MCF) and coupled into the chip with a local oscillator (LO) light. The polarization state of each signal light is automatically adjusted and aligned with that of the LO light, and then 7 channels of 28-GHz MMW carrying 4-Gb/s QPSK signals are generated by optical heterodyne beating. Automated polarization-control function of each channel is also demonstrated with ~7-ms tuning time and ~27-dB extinction ratio.

Key words: multi-channel; millimeter-wave (MMW) generation; silicon photonic integrated circuits; silicon polarization control (SPC)

1. Introduction

To meet the demand for exponentially increasing data traffic in fifth-generation (5G) wireless communications, large-scale antenna array systems operating at millimeter-wave (MMW) frequencies have been intensively studied to support the future broadband mobile networks[1–5]. The MMW frequency band can provide massive amount of underutilized spectrum resources to overcome the bandwidth bottleneck induced by low-frequency wireless carriers[6]. In addition, the short wavelengths of the MMW frequencies enable a small-physical size to pact large number of antennas[7], which are desired for the multi-input multi-output (MIMO) communications. However, due to the large number of antenna elements, realizing large-scale MMW antenna arrays in practical systems faces some challenges in terms of size, weight, hardware cost and power consumption[8–10].

Photonic integrated circuits (PIC) technology, as an alternative approach to implementing high performance MMW antenna systems, has attracted significant interests[11–13]. One motivation is that the MMW generation based on photonic techniques can provide high-quality signals with low phase noise and wide frequency tuning range[14]. PIC technology also opens up attractive possibilities in phased arrays for optical beam steering[15]. Several PIC structures for microwave or MMW signal generation have been demonstrated based on either silicon photonics or III–V photonics to date [16–18]. In Ref. [16], above 100-GHz MMW signals were generated on an InP-based PIC with two distributed feedback lasers integrated on-chip for dual-wavelength heterodyne beating. While in

Ref. [17], the dual-wavelength sources were implemented by an arrayed waveguide grating-based multi-wavelength laser on an InP-based PIC, and 95-GHz MMW carriers were generated. Ref. [18] described a silicon-based PIC for microwave signal generation based on a reconfigurable grating and an integrated optoelectronic oscillator. Ref. [19] demonstrated the generation of up to 60-GHz burst radio frequency waveforms with a silicon photonic chip. For large-scale antenna array systems in 5G multi-user MIMO scenarios, however, a multi-channel MMW generation PIC scheme is highly desirable to distribute multiple user data at the same wireless carrier frequencies based on space multiplexing. On the other hand, silicon photonics has the great potential to offer an integrated solution due to the unique advantages of low fabrication costs, compact size, and compatibility with complementary metal oxide semiconductor (CMOS)[20].

In our previous work[21], we proposed an on-chip silicon-based multi-channel MMW signal generation scheme with heterodyne beating for large-scale antenna arrays. To align the polarization states between the signal lights and the LO lights before heterodyne beating, automated silicon polarization controllers (SPCs) consisting of on-chip polarization control units[22] and off-chip sub-control systems were implemented. Based on the fabricated device, 5 channels of 28-GHz MMW carrying the same 2-Gb/s OOK signals were successfully generated. However, only one channel was wire-bonded to realize on-chip polarization control to verify the feasibility of the control algorithm.

In this paper, we experimentally demonstrated a fully functional 7-channel integrated silicon photonic chip with polarization controls for all the channels. Each channel uses optical heterodyne beating method to generate a 28-GHz MMW carrying a 4-Gb/s QPSK signal for one antenna array in the base station (BS). Then large-capacity MMW signals can be delivered
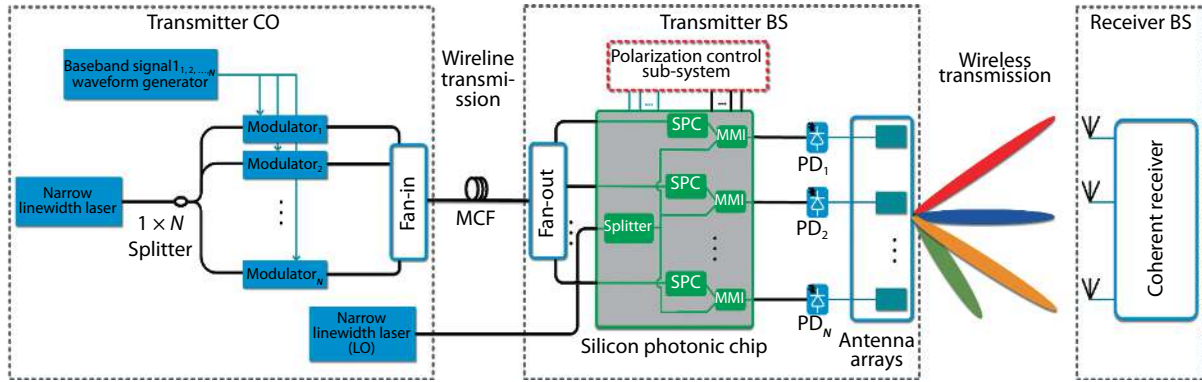
Fig. 1. (Color online) The proposed multi-channel FWI system architecture based on the silicon photonic MMW generator.

by multiple antenna arrays over different wireless links based on the beamforming technology[23]. To transmit multi-channel optical baseband signals at the same optical wavelength, a 2-km 7-core fiber (7CF) is used to perform space-division multiplexing for fronthaul transmissions in the system[24]. The generated QPSK MMW signals are detected and demodulated to retrieve the user data.

2. System architecture and the silicon photonic MMW-generation chip

2.1. System architecture

Fig. 1 shows the schematic architecture of a multi-channel fiber-wireless-integration (FWI) transmission system[25], in which a multi-core fiber is used to perform fronthaul transmission. The proposed silicon photonic integrated circuit is placed at the base station to generate multi-channel MMW signals for large-scale antenna array systems. At the central office (CO), multiple optical baseband signals are generated and delivered at the same wavelength via an MCF. After MCF transmissions, optical baseband signals are coupled into the silicon PIC to generate multiple channels of MMW signals with an identical electrical frequency by heterodyne beating with a LO light. Thus, only a single narrow linewidth laser source is required at the CO. The MMW frequency can be easily varied by tuning the wavelength spacing between the two CW lights. Note that the fiber transmission creates random polarization-state shifts. Thus, silicon polarization controllers (SPCs) are needed to automatically adjust the polarization states of the incoming lights, so they are aligned with that of the LO light. The generated multi-channel MMW signals are distributed to different receiver ends by large-scale antenna arrays over the wireless link.

2.2. Fabricated device and the control sub-system

The micrograph of the fabricated device is shown in Fig. 2(a) with a compact footprint of 1.1×2.1 mm^2. It implements the SPC for each channel to align the polarization states of the input signal light and that of the LO light. The schematic of the on-chip polarization control units is depicted in Fig. 2(b). The SPC structure was proposed in Ref. [22] to realize an automated polarization receiver in an integrated silicon photonic circuit. At the input port, a polarization splitter and rotator (PSR)[26] is adopted to divide the TE light and the TM light of the signal, and simultaneously rotate the TM portion to a TE polarized light. Then a balanced Mach–Zehnder interferometer

(MZI) with two micro heaters and two 2×2 multi-mode interferometers (MMIs) are employed to control the phases and amplitudes of the two lights, which are transmitted to the output port and the monitoring port, respectively. At the monitoring port, the optical power is converted to electrical signal and then amplified, sampled and processed by the control sub-system. Using the transfer matrix method[27], the monitored power as a function of the phase tunings of the two micro heaters denoted as $\Delta\phi_1$ and $\Delta\phi_2$ can be written as

$$P_M(\Delta\phi_1, \Delta\phi_2) = \left| a\left[e^{-j(\phi_1+\Delta\phi_1+\Delta\phi_2)} - e^{-j(\phi_1+\Delta\phi_1)}\right]/2 \right.$$
$$\left. + b\left[e^{-j(\phi_2+\Delta\phi_2-\pi/2)} + e^{-j(\phi_2-\pi/2)}\right]/2 \right|^2,$$

where a and b represent the intensities of the two input lights of the first MMI respectively, and $a^2 + b^2 = 1$; while ϕ_1 and ϕ_2 are the initial phase of the two input lights. Normalized $P_M(\Delta\phi_1, \Delta\phi_2)$ with different optical power ratios and initial phase differences between the two inputs of the first MMI are numerically calculated and shown in Fig. 2(c). It is observed that $P_M(\Delta\phi_1, \Delta\phi_2)$ has two centro-symmetric global minimum points, which means we can reduce the monitored optical power to one of the global minimum points by calculating and setting the proper phase tunings of the two micro-heaters. Then a power-maximized TE polarized signal light at the output port can be obtained. Note that the polarization state of the LO light after vertical coupling is TE-mode due to the TE grating, thus the polarization state of each channel of signal lights is aligned with that of the LO light. Figs. 2(d) and 2(e) show the photograph and schematic of the control sub-system for automated polarization control, respectively. In the control sub-system, each channel of the monitoring lights is sent into a photodetector for optical-to-electrical conversion. Then a trans-impedance amplifier (TIA) is used to amplify the photocurrent signal. The 7 channels of monitored electrical signals are then sampled by analog-to-digital converter (ADC) arrays and sent to a centralized processor. A global minimum-power searching algorithm is then designed and employed in the centralized processer to minimize the monitored optical power at each monitoring port. Different from the polarization control algorithm in Ref. [22], which searches for the minimum power at the feedback port by gradient descent method, the proposed algorithm uses an optimized minimum searching strategy to avoid the affection of the local minima.

Fig. 3 illustrate the pseudo-code of the algorithm, which consists of two minimum-power searching sub-processes in or-
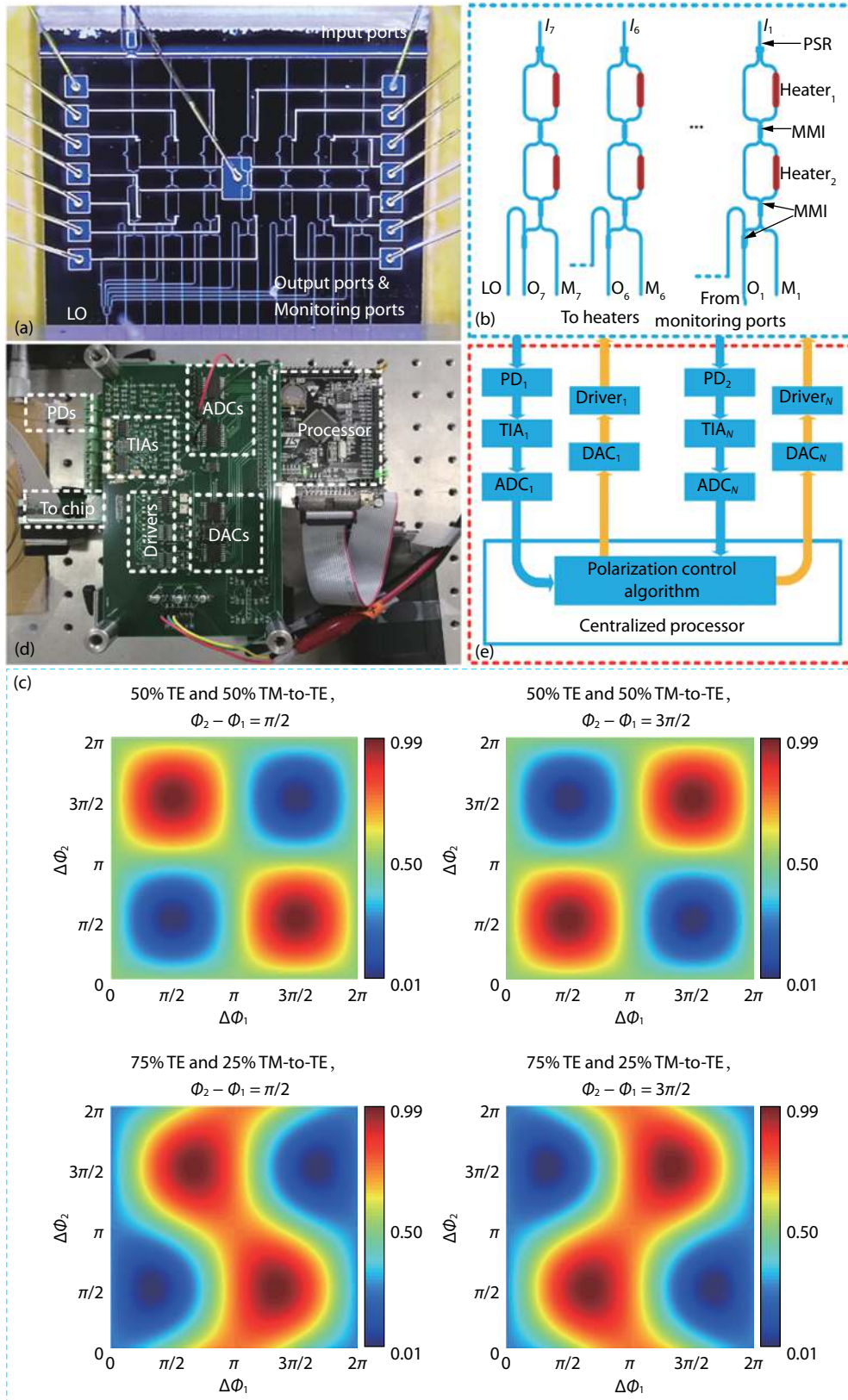
Fig. 2. (Color online) (a) Micrograph of the fabricated chip. (b) Schematic diagrams of the polarization tuning units. (c) Normalized $P_M(\Delta\phi_1, \Delta\phi_2)$ with different optical power ratios and initial phase differences between the two inputs of the first MMI. (d) Photograph of the polarization control sub-system. (e) Schematic diagram of the control sub-system.

der during one iteration. The minima of P_M during the two sub-processes are denoted as P_{M_min1} and P_{M_min2}, respectively. In sub-process (1), $\Delta\phi_1$ is tuned to search for P_{M_min1} with a tuning range of 2π. Then in sub-process (2), $\Delta\phi_2$ is tuned to fur-

ther reduce the monitored optical power to approach the global minimum. P_1 and P_2 are the thermal tuning powers applied on the two micro heaters. By tuning one micro heater over a large phase-shift range at a time instead of switching between

Fig. 3. (Color online) Pseudo-code of the global minimum-power searching algorithm.
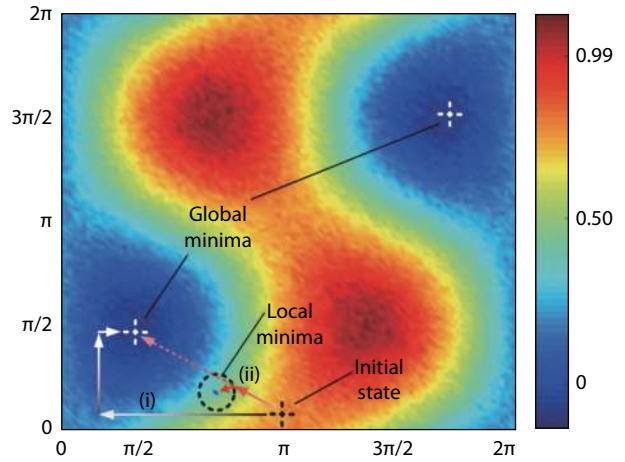

Fig. 4. (Color online) Progresses of the proposed algorithm and the algorithm in Ref. [22] when a local minima exists in the normalized $P_M(\Delta\phi 1, \Delta\phi 2)$ with a 75% to 25% power ratio and a π/2 phase difference between the two inputs of the first MMI.
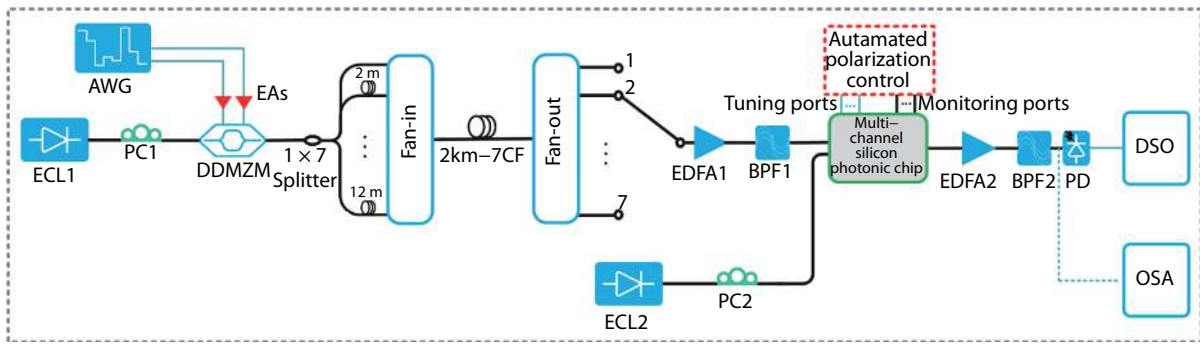

Fig. 5. (Color online) Experimental setup of the multi-channel MMW signals generation base on the proposed silicon photonic MMW generator.

the two micro heaters with small steps, the proposed algorithm can effectively prevent the tuning process being trapped into local minima where the monitored signal is buried in noise. Fig. 4 shows this situation, where a local minima exists in the normalized $P_M(\Delta\phi_1, \Delta\phi_2)$ with a 75% to 25% power ratio and a π/2 phase difference between the two inputs of the first MMI. Path (i) and path (ii) represent the tuning directions of our global minimum-power searching strategy and the gradient descent strategy in Ref. [22], respectively. When the local minima locate near the path from the initial state to one of the global minima, the gradient descent progress will fall into it, while our proposed algorithm would not. In practice, usually one iteration can finely obtain a desired extinction ratio between the output optical power and the monitored optical power. After automated polarization control by the SPC, the signal light is mixed with the LO light by an MMI and then sent to a broadband PD to generate a MMW signal.

3. Experimental setup and results

To verify the feasibility of the proposed integrated multi-channel MMW signal generator, we perform a proof-of-concept experiment with an experimental setup shown in Fig. 5. At the CO, a CW light at 1550.230 nm from a free-running external cavity laser denoted as ECL1 (Koheras BASIK C15), with a <15-kHz linewidth and 10-dB output optical power is fed into a 25-GHz

dual-drive Mach–Zehnder modulator (DDMZM) (T.DKH1.5-40PD-ADC). The DDMZM biased at the quadrature point is driven by two 2-Gb/s pseudo-random bit sequence (PRBS) streams with the same word length of $2^{11}-1$, producing a 2-Gbaud QPSK optical baseband signal. The two electrical baseband signals are generated by an arbitrary waveform generator (AWG) (Keysight M8195A) with a sampling rate of 60-GSa/s and then amplified by two parallel electrical amplifiers (EAs). Note that the baseband signal is resampled to mitigate the sidelobes and therefore minimize the occupied bandwidth. The output optical baseband signal form the DDMZM is divided into 8 channels by a 1 × 8 splitter with ~11-dB single-path insertion loss, and 7 channels are used and fed into different cores of a 2-km 7-core fiber (7CF). The intra-channel crosstalk between adjacent cores is less than −50 dB and the insertion loss of each core is ~ 4.25 dB. Channel decorrelation is carried out by using 7 single-mode fibers (SMFs) with a 2-m interval to ensure that the optical baseband signals in different cores of the 7CF are totally uncorrelated[28]. After the 7CF transmission, each channel of the baseband signal lights is boosted by an erbium-doped fiber amplifier (EDFA) with a ~21-dB amplification gain. The output signal light of the EDFA is coupled into the multi-channel silicon MMW generator by an edge coupler with a ~5-dB coupling loss. In the experiment, only one channel of signal is tested at a time due to the lack of EDFA and fiber-array
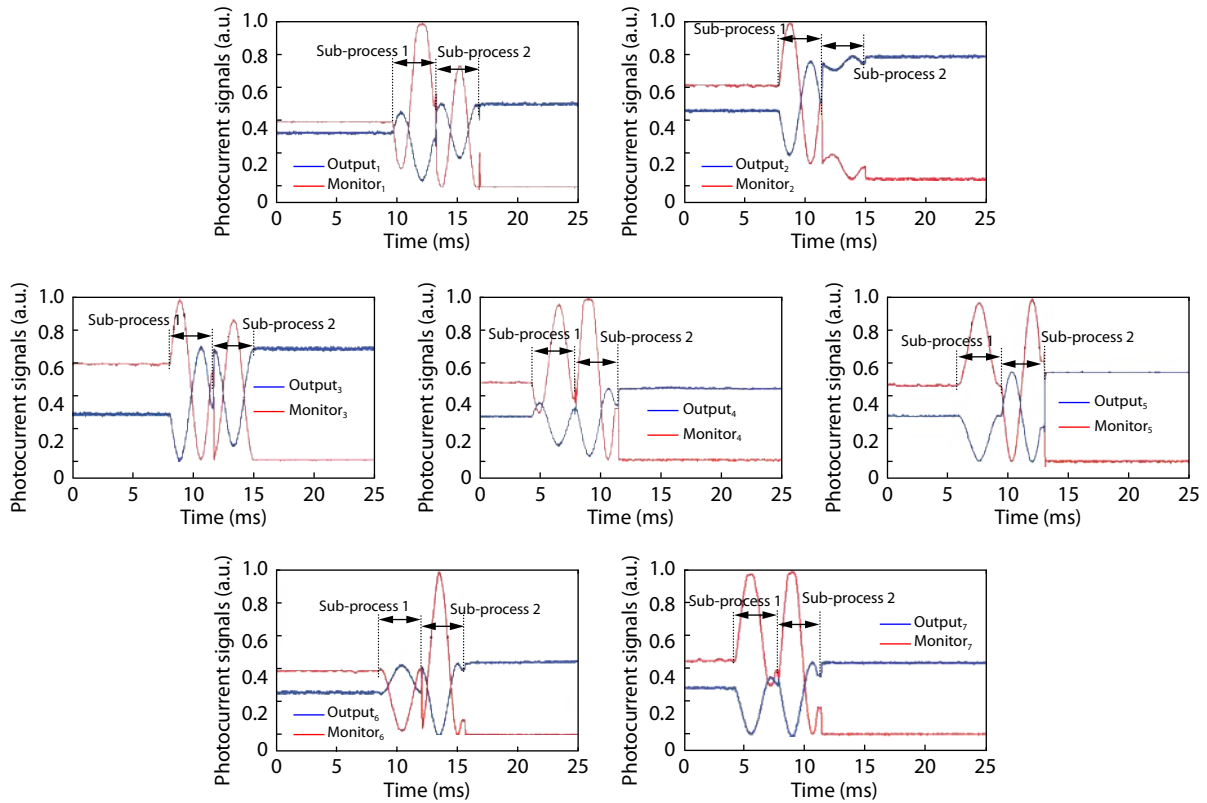
Fig. 6. (Color online) On-chip automated polarization-tuning progresses of the 7-channel signal lights.

for edge coupling. A CW light at 1550.010 nm, generated from another free-running ECL (denoted as ECL2) with <15-kHz linewidth, is employed as an optical LO for on-chip dual-wavelength heterodyne beating. The LO light has a 28-GHz frequency spacing from the signal light and is injected into the LO port of the chip by vertical coupling with a ~9 dB power loss. On-chip automated polarization tuning progresses of the 7 channels of signal lights are demonstrated in Fig. 6, which plots the normalized photocurrent waveforms at the monitoring ports and the output ports versus time. In the experiment, optical power at the monitoring port and the output port of each channel are firstly converted to electrical signals by two PDs and amplified by two TIAs. Then a dual-channel digital storage oscilloscope (DSO) (Tektronix TBS1002) with a 1-GSa/s sampling rate and a 100-MHz bandwidth is used to capture the photocurrent signals in the progress of automated polarization tuning. As shown in Fig. 6, after executing the two sub-processes, the optical power at the output ports are maximized while the optical power at the monitoring ports are minimized. Note that the optical power at the monitoring port is ~3-dB higher than that at the output port due to an MMI at the output port for mixing. For each channel, ~27-dB extinction ratio between the output optical power and the monitoring optical power and a ~7-ms polarization tuning time are achieved, which is fast enough to adapt to the random polarization-state shift caused by the fiber transmission. By employing the improved searching strategy proposed in Ref. [29] that consists of the coarse scanning process and the fine scanning process, the polarization tuning time can be further reduced.

After the automated polarization tuning for each channel, the signal light and the LO light are combined by the MMI at the output port and coupled out of the chip by vertical coupling. All the vertical coupling ports are connected to a fiber ar-

ray coupler. The output signal light of one tested channel is then amplified by an EDFA, filtered by an optical bandpass filter (BPF) with a 1-nm bandwidth and detected by a 40-GHz PD (XPDV2120R) to generate a ~28-GHz MMW signal. Before the PD, an optical spectrum analyzer (OSA) (APEX 2040C) with a 1.12-pm resolution is used to record the optical spectrum of the mixed signal, so the powers of the two signals are approximately known. To match the powers of the two lights, the amplification gain of the second EDFA can be adjusted such that the power of the signal light equals to that of the LO light, based on the real-time measurements of the OSA. At the output of the PD, we sample the MMW signal by an 80-GSa/s DSO (LeCroy 10-36Zi-A) and demodulate the baseband QPSK data by offline digital signal processing (DSP), including carrier recovery, down-conversion, symbol synchronization, and signal-to-noise ratio (SNR) measurement. Note that a 28-GHz RF source can perform the demodulation and significantly lower the requirement of the sampling rate. Fig. 7(a) shows the waveforms and the demodulated constellation diagrams of the generated 7-channel QPSK MMW signals. The optical spectrum and the electrical spectrum of channel 1 before and after heterodyne beating are illustrated in Figs. 7(b) and 7(c), respectively. The other channels show similar optical and electrical spectra. Fig. 7(d) gives the SNR performances of the 7 channels of demodulated QPSK signals, which is calculated by the following equation[30]:

$$\mathrm{SNR} = 10\log_{10}\left(\frac{\sum_{n=1}^{N}(I_K^2 + Q_K^2)}{\sum_{n=1}^{N}\left((I_K - X_K)^2 + (Q_K - Y_K)^2\right)}\right),$$

where N is the symbol number, I_k and Q_k represent in-phase amplitude and quadrature amplitude of the kth reference
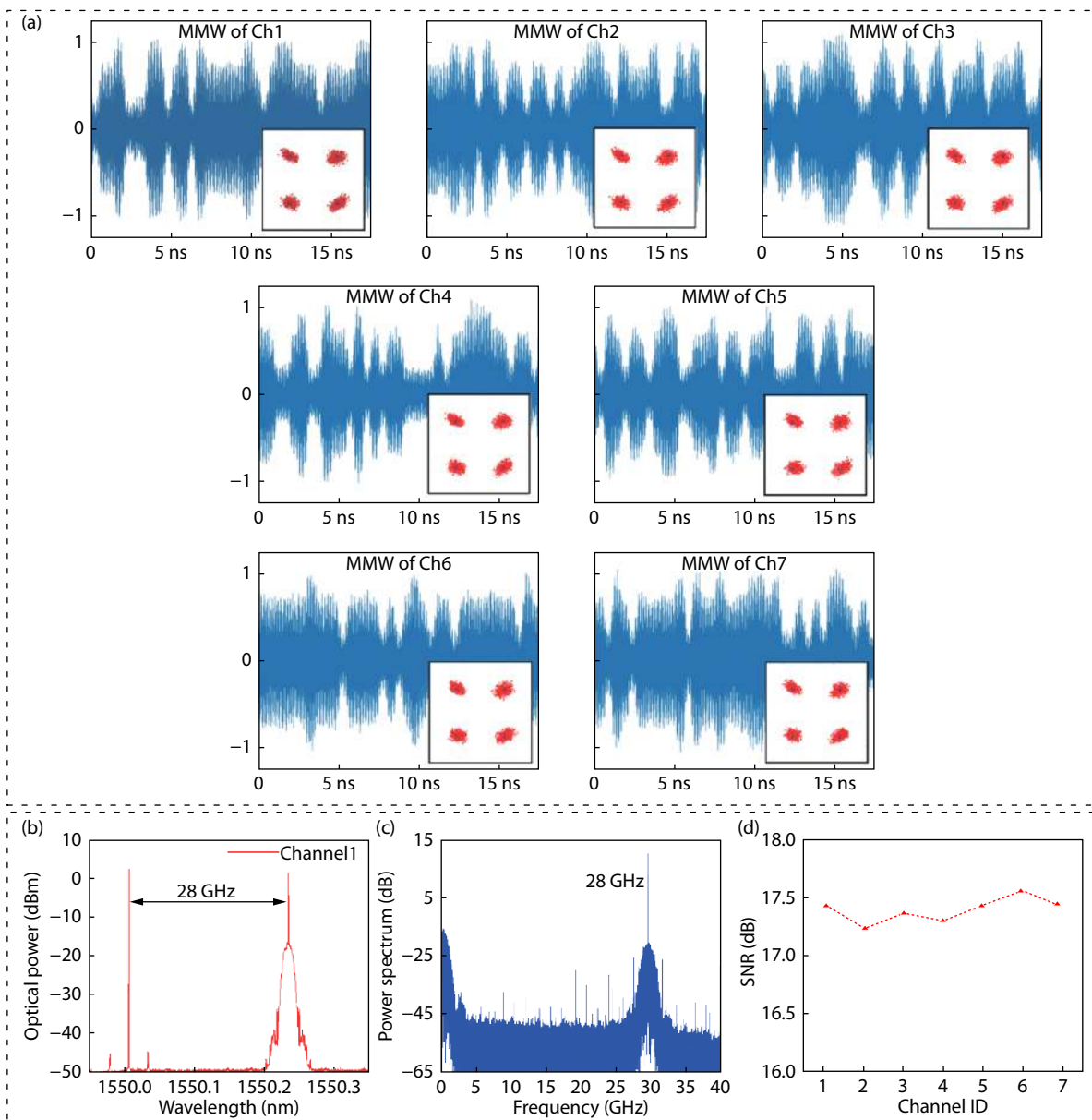
Fig. 7. (Color online) (a) Waveforms and the demodulated constellation diagrams of the generated 7-channel QPSK MMW signals. (b) Optical spectrum of channel-1 of the MMW signal before the heterodyne beating. (c) Electrical spectrum of channel-1 of the MMW signal after the heterodyne beating. (d) Measured SNRs of the 7 channels of demodulated QPSK signal.

QPSK symbol, respectively, and X_k, Y_k are the in-phase amplitude and quadrature amplitude of the kth received QPSK symbol, respectively.

4. Conclusion

In summary, we have proposed a silicon PIC scheme to generate multi-channel MMW signals for large-scale antenna array systems. We have experimentally demonstrated a FWI system, with a 2-km 7CF used as fronthaul transmission of different optical baseband signals, and 7 channels of 28-GHz MMW carrying 4-Gb/s QPSK signals generated in the BS. The MMW signals are demodulated with the best SNR of 17.6 dB. Automated silicon polarization controllers are also implemented with ~7-ms tuning time and ~27-dB extinction ratio.

References

[1] Agiwal M, Roy A, Saxena N. Next generation 5G wireless networks: A comprehensive survey. IEEE Commun Surv Tut, 2016, 18(3), 1617

[2] Han S F, I C L, Xu Z K, et al. Large-scale antenna systems with hybrid analog and digital beamforming for millimeter wave 5G. IEEE Commun Mag, 2015, 53(1), 186

[3] Pi Z, Khan F. An introduction to millimeter-wave mobile broadband systems. IEEE Commun Mag, 2011, 49(6), 101

[4] Sulyman A I, Nassar A T, Samimi M K, et al. Radio propagation path loss models for 5G cellular networks in the 28 GHz and 38 GHz millimeter-wave bands. IEEE Commun Mag, 2014, 52(9), 78

[5] Roh W, Ji-Yun Seol J Y, Park J, et al. Millimeter-wave beamforming as an enabling technology for 5G cellular communications:

Theoretical feasibility and prototype results. IEEE Commun Mag, 2014, 52(2), 106

[6] Rappaport T S. Millimeter wave mobile communications for 5G cellular: It will work!. IEEE Access, 2013, 1(1), 335

[7] Heath R W. An overview of signal processing techniques for millimeter wave MIMO systems. IEEE J Sel Top Signal Process, 2016, 10(3), 436

[8] Gao X, Dai L, Sayeed A M. Low RF-complexity technologies to enable millimeter-wave MIMO with large antenna array for 5G wireless communications. IEEE Commun Mag, 2018, 56(4), 211

[9] Rebeiz G. Millimeter-wave large-scale phased-arrays for 5G systems. Microwave Symposium (IMS), IEEE MTT-S International, 2015, 1

[10] Gao X. Energy-efficient hybrid analog and digital precoding for mm-Wave MIMO systems with large antenna arrays. IEEE J Sel Areas Commun, 2016, 34(4), 998

[11] Li M. Harnessing optical forces in integrated photonic circuits. Nature, 2008, 456(7221), 480

[12] Marpaung D. Integrated microwave photonics. Laser Photonics Rev, 2013, 7(4), 506

[13] Zhang W, Yao J. Silicon-based integrated microwave photonics. IEEE J Quantum Electron, 2016, 52(1), 1

[14] Guzmán R, Carpintero G, Gordon C, et al. Millimeter-wave signal generation for a wireless transmission system based on on-chip photonic integrated circuit structures. Opt Lett, 2016, 41(20), 4843

[15] Amato F, Serafino G, Ghelfi P. Ultra-fast beam steering of a phased-array antenna based on packaged photonic integrated circuits. IEEE European Conference on Optical Communication (ECOC), 2018, Tu3H

[16] Carpintero G. Microwave photonic integrated circuits for millimeter-wave wireless communications. IEEE/OSA J Lightw Technol, 2014, 32(20), 3495

[17] Carpintero G. 95 GHz millimeter wave signal generation using an arrayed waveguide grating dual wavelength semiconductor laser. Opt Lett, 2012, 37(17), 3657

[18] Yao J. Photonic integrated circuits for microwave signal generation and processing. Conference on Lasers and Electro-Optics (CLEO), 2018, JTh4D.1

[19] Khan M H. Ultrabroad-bandwidth arbitrary radiofrequency waveform generation with a silicon photonic chip-based spectral shaper. Nat Photon, 2010, 4(2), 117

[20] Yao J. Microwave photonics. IEEE/OSA J Lightw Technol, 2009, 27(3), 314

[21] Cao R Y, He Y, Yao J P. Integrated multi-channel millimeter wave photonic generation based on a silicon chip with automated polarization control. IEEE European Conference on Optical Communication (ECOC), 2018, We2.43

[22] Ma M L, Murray K, Ye M Y, et al. Silicon photonic polarization receiver with automated stabilization for arbitrary input polarizations. Conference on Lasers and Electro-Optics (CLEO), 2016, STu4G.8

[23] Zhu M, Zhang L, Wang J, et al. Radio-over-fiber access architecture for integrated broadband wireless services. IEEE/OSA J Lightw Technol, 2013, 31(23), 3614

[24] Macho A. Next-generation optical fronthaul systems using multicore fiber media. IEEE/OSA J Lightw Technol, 2016, 34(20), 4819

[25] Kanno A, Dat P T, Kuri T, et al. Evaluation of frequency fluctuation in fiber-wireless link with direct IQ down-converter. IEEE European Conference on Optical Communication (ECOC), 2017, We.3.6.3

[26] Tan K. Ultra-broadband fabrication-tolerant polarization splitter and rotator. Optical Fiber Communication Conference, 2017, Th1G.7

[27] Yariv A. Critical coupling and its control in optical waveguide-ring resonator systems. IEEE Photon Technol Lett, 2002, 14(4), 483

[28] Luo L. WDM-compatible mode-division multiplexing on a silicon chip. Nat Commun, 2014, 5, 3069

[29] Zhu Q, et al. Wide-range automated wavelength calibration over a full FSR in a dual-ring based silicon photonic switch. Optical Fiber Communication Conference (OFC), 2018, Th3C.1

[30] Bergano N S, Kerfoot F W, Davidsion C R. Margin measurements in optical amplifier system. IEEE Photon Technol Lett, 1993, 5(3), 304